

## Supporting Information

# Palladium-Decorated Hydrogen-Gas Sensors Using Periodically Aligned Graphene Nanoribbons

*By Yusin Pak, Sang-Mook Kim, Huisu Jeong, Chang Goo Kang, Jung Su Park, Hui Song, Ryeri Lee, NoSung Myoung, Byoung Hun Lee, Sunae Seo, Jin Tae Kim<sup>\*</sup>, Gun-Young Jung<sup>\*</sup>*

<sup>\*</sup> School of Materials Science and Engineering  
Gwangju Institute of Science and Technology (GIST)  
261 Cheomdan-gwagiro(Oryong-dong)  
Buk-gu, Gwangju 500-712, Republic of Korea  
E-mail: gyjung@gist.ac.kr

## S1. Comparative table and graphs for sensitivities and response times of various Pd-based sensors

We surveyed the previous studies dealing with Pd-based sensors, such as Pd films and Pd nanowires. The characteristics of Pd film- and Pd nanowire-based sensors are summarized in a table below. Both Pd film- and Pd nanowire-based hydrogen gas sensors show relatively low sensitivities at a low level concentration.

**Table S1.** Previous reports on Pd film- and Pd nanowire-based hydrogen gas sensors.

Ref.	Type	Sensitivity	Response time	Ambient
(1) Thin Solid Films, 519, 880-884	Film	~1.5 % ( $3 \times 10^3$ ppm), ~3 % ( $1.4 \times 10^4$ ppm)	(36.8 %) ~5 s ( $10^4$ ppm)	N <sub>2</sub>
(2) Nanotechnology, 20, 015502	Film	~2 % ( $5 \times 10^3$ ppm), ~22 % ( $5 \times 10^4$ ppm)	(90 %) ~45 s	N <sub>2</sub>
(3) Appl. Phys. Lett., 86, 203104	Film	~30 % ( $10^4$ ppm)	(90 %) ~68 ms ( $2 \times 10^4$ ppm)	N <sub>2</sub>
(4) Appl. Phys. Lett., 94, 223110	NW	~1.5 % ( $10^3$ ppm), ~4 % ( $10^4$ ppm)	(90 %) ~30 s (27 ppm)	Air
(5) Nanotechnology, 20, 135502	NW	~0.37 % (500 ppm), ~3.83 % ( $10^4$ ppm)	(36.8 %) ~8.4 s (500 ppm)	N <sub>2</sub>
(6) Small, 6, No. 13, 1422-1429	NW	~0.5 % (50 ppm), ~20 % ( $4 \times 10^4$ ppm)	Unwritten	N <sub>2</sub>
(7) Small, 2, No. 3, 356-358	NW	~0.34 % (200 ppm), ~1.27 % ( $10^5$ ppm)	Unwritten	N <sub>2</sub>

Comparative studies were made with various Pd-based hydrogen sensors we surveyed (from 26 papers). Two graphs can be drawn, demonstrating sensitivity and response time vs. gas concentration in the various Pd-based hydrogen sensors. Most sensors have sensitivities of below 30 % regardless of hydrogen concentration. It is noteworthy that the Pd film-based sensors are working at a high concentration of over 1000 ppm.

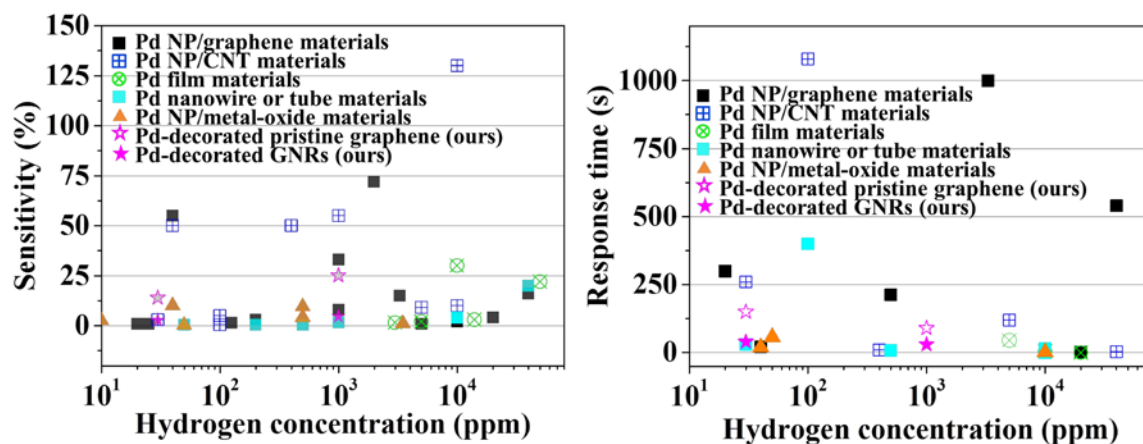


**Figure S1.** Comparison of sensitivity and response time at different concentration from various Pd-based hydrogen gas sensors.

(References for Table S1)

- (1) Lee, E.; Lee, J. M.; Lee, E.; Noh, J.-S.; Joe, J. H.; Jung, B.; Lee, W. Hydrogen Gas Sensing Performance of Pd-Ni alloy Thin Films. *Thin Solid Films* **2010**, *519*, 880–884.
- (2) Khanuja, M.; Kala, S.; Mehta, B. R.; Kruis, F. E. Concentration-specific hydrogen sensing behavior in mesosized Pd nanoparticle layers. *Nanotechnology* **2009**, *20*, 015502.
- (3) Xu, T.; ZaCh, M. P.; Xiao, Z L.; Rosenmann, D.; Welp, U.; Kwok, W. K.; Crabtree, G. W. Self-Assembled Monolayer-Enhanced Hydrogen Sensing With Ultrathin Palladium Films. *Appl. Phys. Lett.* **2005**, *86*, 203104.
- (4) Offermans, P.; Tong, H. D.; Van Rijn, C. J. M.; Merken, P.; Brongersma, S. H.; Crego-Calama, M. Ultralow-Power Hydrogen Sensing With Single Palladium Nanowires. *Appl. Phys. Lett.* **2009**, *94*, 223110.
- (5) Jeon, K. J.; Lee, J. M.; Lee, E.; Lee, W. Individual Pd Nanowire Hydrogen Sensors Fabricated by Electron-Beam Lithography. *Nanotechnology* **2009**, *20*, 135502.
- (6) Yang, F.; Taggart, D. K.; Penner, R. M. Joule Heating a Palladium Nanowire Sensor for Accelerated Response and Recovery to Hydrogen Gas. *Small* **2010**, *6*, 1422–1429.
- (7) Im, Y.; Lee, C.; Vasquez, R. P.; Bangar, M. A.; Myung, N. V.; Menke, E. J.; Penner, R. M.; Yun, M. Investigation of a Single Pd Nanowire for Use as a Hydrogen Sensor. *Small* **2006**, *2*, 356–358.

## S2. Pattern transfer from PR line mask to Cr film.

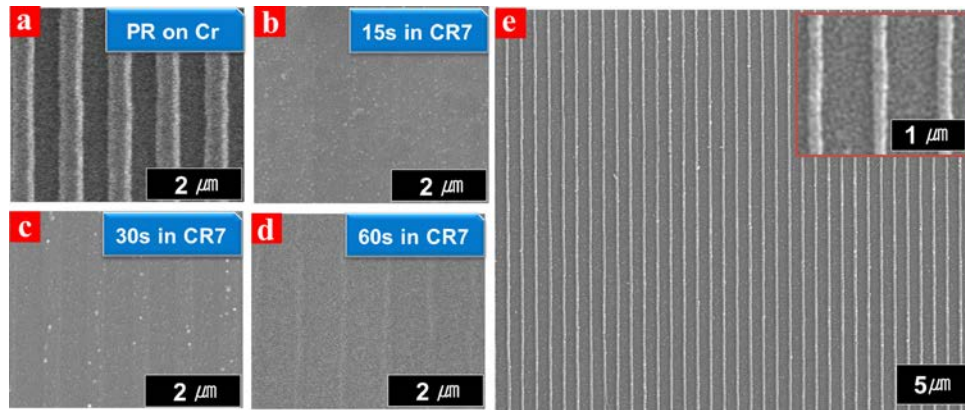


**Figure S2.** SEM images of (a) the PR line pattern on the Cr/graphene layer, (b~d) the transferred Cr line pattern etched with different wet-etching times after PR stripping and (e) the SiO<sub>2</sub> line pattern obtained after CF<sub>4</sub> plasma etching using the Cr line mask of Figure S2(d).

The AZ GXR 601 positive tone PR line pattern with a 500 nm linewidth at 1 μm pitch was fabricated by 325 nm He-Cd laser interference lithography as shown in S2(a). To transfer the patterns to the underlying Cr layer, the sample was dipped into a CR-7 etchant with different times (15, 30 and 60 sec) to determine the optimum etching time. The PR was then removed, revealing the transferred Cr line pattern as shown in Figure S2(b, c and d). After 15 sec of etching, Cr was still remained in the gaps. After 30 sec, the Cr line pattern was clear and had a similar width to the PR pattern. After 60 sec, the Cr line pattern was over-etched and shrunken. In our experiment, 40 sec etching, hence slight over-etching, was used to ensure no Cr residue remained at the gaps. If the Cr is remained, the subsequent graphene patterns would have defects or, in the extreme case, no line pattern would be transferred. Using the Cr line mask of Figure S2(d), the underlying SiO<sub>2</sub> was etched with CF<sub>4</sub> plasma, creating separate and continuous SiO<sub>2</sub> lines across a large area as shown in Figure S2(e).

### S3. Raman spectra of the GNR array with/without the PR residue

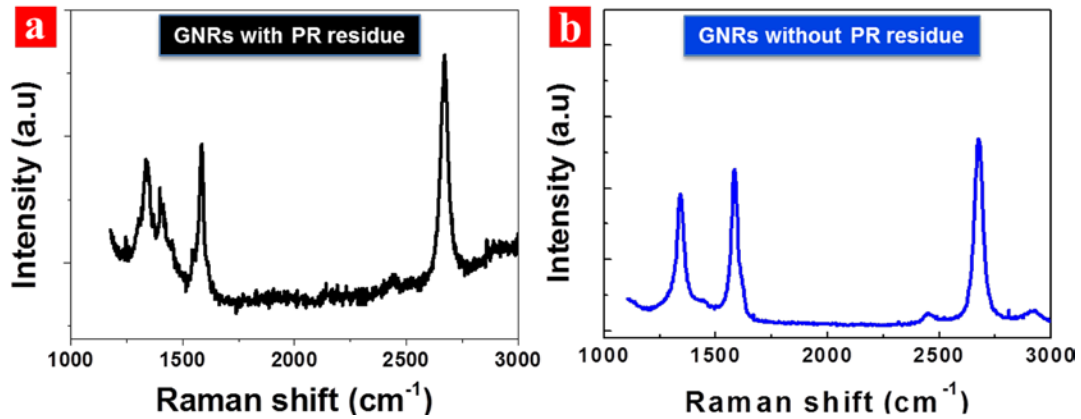
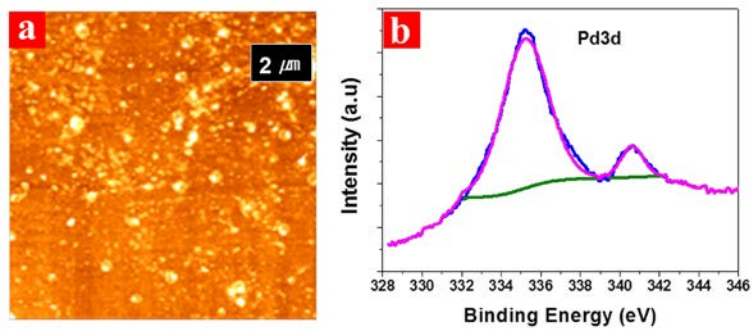


Figure S3(a) shows the Raman spectrum of GNRs contaminated with PR residue, evidenced by a peak between the D and G bands of graphene. As explained in the text, the GNR array of Figure S3(a) was fabricated by spin-coating PR directly onto the graphene surface before performing the laser interference lithography. The  $1406\text{ cm}^{-1}$  peak overlapping with the D and G bands of graphene is caused by PR residue. In contrast, the GNRs of Figure S3(b) array produced by utilizing the Cr interlayer has a much-reduced peak at  $1406\text{ cm}^{-1}$  between the D and G bands.

#### S4. Palladium deposition and its characterization



**Figure S4.** (a) AFM image and (b) XPS spectrum of the palladium nanoparticles.

Palladium was deposited by electron beam evaporation with a set thickness of 2 nm. It was not electrically connected, but stayed as nanoparticles or little islands as shown in Figure S4(a). X-ray photoelectron spectroscopy confirmed the presence of palladium nanoparticles at two peaks at 335.01 eV and 340.87 eV, well matched with the typical palladium XPS peaks.

## S5. Gas sensitivity measurement setup



**Figure S5.** Homemade setup for gas sensitivity measurement

Figure S5 shows our homemade setup for measuring gas sensitivity. The setup is divided into four parts; (1) resource: gas and regulators, (2) injector: mass flow controller, readout system, gas mixer, (3) chamber: 2 inch quartz tube and temperature controller and (4) analyzer: Keithley 2400 and homemade Lab-VIEW resistance analyzing program.

**S6. Response and recovery time for 40 %, 60 % and 80 % performance of both pristine and GNR sensors**

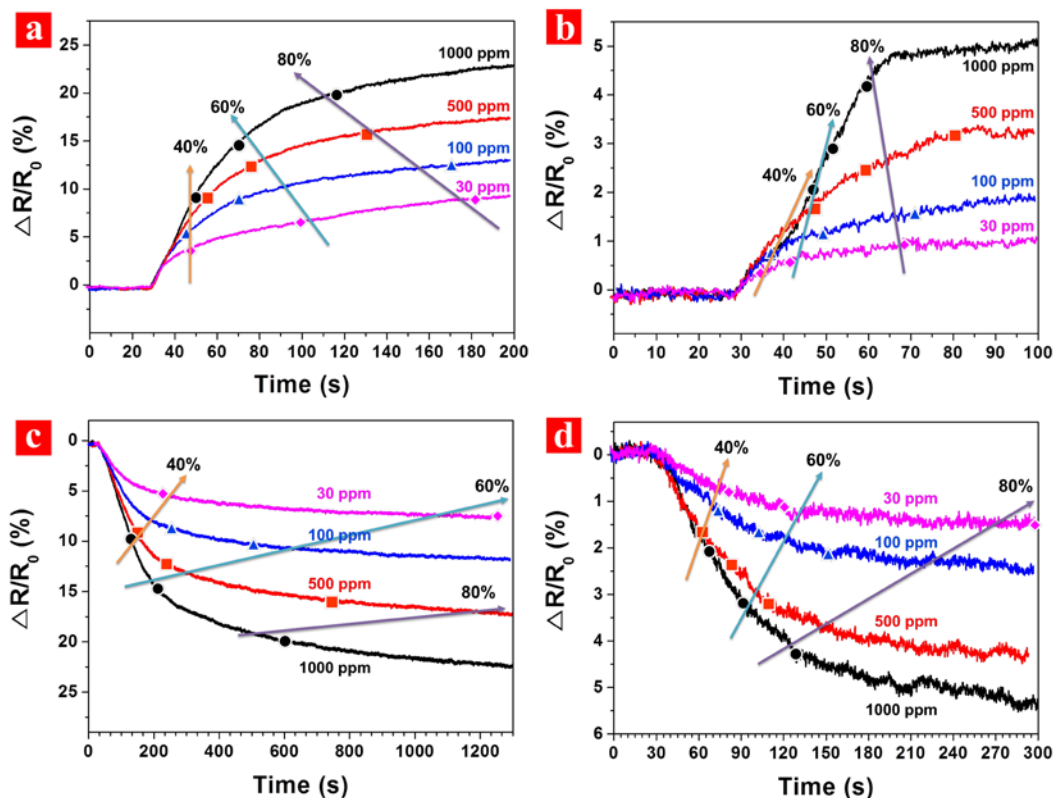


**Figure S6.** (a, b) Response time for reaching 40 %, 60 % and 80 % of the saturated sensitivity and (c, d) the recovery time for returning 40 %, 60 % and 80 % recovery to the initial ground current at various concentrations. [(a, c): pristine, (b, d): GNR array sensor]

Figure S6 shows the response and recovery behavior of both Pd-decorated pristine and GNR sensors at various concentrations. The time taken to reach 40 %, 60 %, and 80 % of the saturated sensitivity for response and the time taken for 40 %, 60 % and 80 % recovery to initial ground current at various concentrations are marked in the figure, and the trend at each percentage is shown with an arrow. In the pristine graphene sensor of Figure S6(a), the arrows head towards left as sensitivity increases, indicating that reaction rate strongly depends on the concentration. In contrast, in the GNR sensor of Figure S6(b), the arrows have a tendency to head towards right, showing that concentration has no significant effect on the gas response for this nanoscale active

area. The same is true for the recovery phenomena of both sensors; the recovery rate in the pristine sensor (Figure S6(c)) strongly depends on the concentration, meanwhile the GNR sensor (Figure S6(d)) is negligibly influenced by the concentration (the GNR sensor has almost vertical arrows, considering the time scale).